Microwave Studies of Self-Aligned Top-Collector Charge Injection Transistors

G. L. Belenky, P. A. Garbinski, P. R. Smith, S. Luryi, A. Y. Cho, R. Hamm, and D. L. Sivco

AT&T Bell Laboratories, Murray Hill, NJ 07974

Abstract

Charge injection transistors have been implemented in molecular-beam-epitaxy-grown InGaAs/InAlAs/InGaAs and InGaAs/InP/InGaAs heterostructures using a self-aligned process for the collector stripe definition. Scattering parameters have been measured in the frequency range from 100 MHz to 40 GHz. InP-barrier devices show the best microwave performance ever reported for a real-space transfer transistor: at 40 GHz the short circuit current gain $|h_{21}|$ is 8 dB and the power gain is larger than unity. The slope of $|h_{21}(f)|$ depends on the bias point and is generally gentler than 20 dB/dec. Extrapolating at the measured slope, we find $|h_{21}|=1$ at $f=115\,\text{GHz}$. The short circuit current gain cutoff f_T, defined by extrapolation at 20 dB/dec from the point of least mean square deviation of the measured slope from 20 dB/dec is $f_T=73\,\text{GHz}$.

Introduction

The charge injection transistor [1] or CHINT is a three-terminal heterojunction device based on the real-space transfer (RST) of hot electrons between two conducting layers. The heating electric field along the *emitter* channel, which plays the role of a hot-electron cathode, is provided by the voltage between "*source*" and "*drain*" electrodes. The other, "*collector*", layer is separated from the emitter by a heterojunction barrier and is contacted separately.

Microwave properties of CHINT have been studied experimentally [2-5] in several material systems (GaAs/AlGaAs [2], InGaAs/InAlAs [3], strained-layer InGaAs/AlGaAs/GaAs [4,5]) and theoretically, using Monte Carlo simulations [6-8]. The ultimate frequency performance of the device is believed to be limited by the time of flight of hot electrons over high-field regions of the device, i.e., over distances of order the barrier-layer thickness. Recent experimental study [5], subsequently supported by MC simulations [7], showed that the intrinsic f_T of CHINT with the collector width of $L_{CH} \approx 1\ \mu m$ is about 3 times higher than that of the FET with the same gate width.

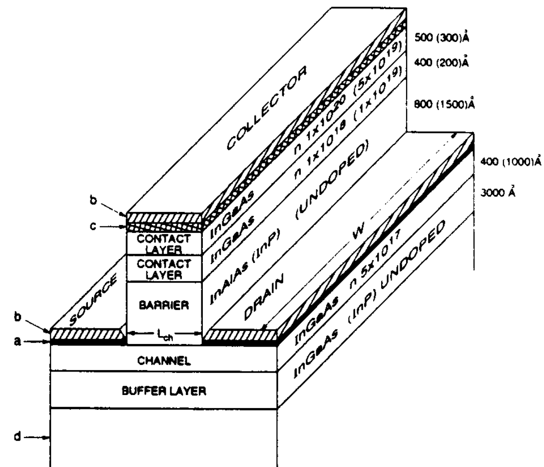

Fig. 1: Schematic diagram of the collector-up charge injection transistors. Letters and numbers in parentheses refer to InP-barrier device. *a*: 450 Å Ni/Ge/Au/Ag/Au alloyed channel contact; *b*: 3000 Å Si_3N_4 layer; *c*: 2000 Å Au collector contact; *d*: semi-insulating InP substrate.

Previously reported high-speed RST transistors have been implemented in either collector-down [2,3] or collector-up [4,5] configuration. Collector-down devices have an unavoidable overlap between the source/drain regions and the collector layer which give rise to parasitic capacitances and limit the microwave performance. The best reported f_T in a down-collector CHINT was 40 Ghz (with MAG > 1 at the highest measured frequency of 25 GHz) obtained in a InGaAs/InAlAs heterostructure with a 2,000 Å-thick InAlAs barrier [3]. Collector-up configurations offer significant advantages in that the parasitic capacitances can be effectively eliminated by patterning the collector stripe. The highest reported frequencies in a collector-up CHINT [4] were $f_T = 60\,\text{GHz}$ (obtained by extrapolating the data measured up to 25 GHz) and a lower $f_{max} = 18\,\text{GHz}$ (presumably due to parasitic resistances in a non-self-aligned structure).

This is the first report of the microwave performance of a self-aligned top-collector CHINT, implemented in MBE-

0-7803-1450-6 $3.00 © 1993 IEEE

grown heterostructures, lattice-matched to InP. Our self-aligned process has been previously used in the implementation of a complementary light-emitting CHINT [9]. We have studied both InAlAs and InP barrier devices. The use of an InP barrier is reported for the first time in a unipolar CHINT; these devices also show the best microwave performance ever reported for a RST transistor.

Experimental Results

The $In_{0.53}Ga_{0.47}As/In_{0.52}Al_{0.48}As/In_{0.53}Ga_{0.47}As$ structure was grown by molecular beam epitaxy (MBE) and the $In_{0.53}Ga_{0.47}As/InP/In_{0.53}Ga_{0.47}As$ by metallorganic MBE (MOMBE). Details of the growth and processing have been described elsewhere [9]. We used optical lithography and selective wet etching. The device structure is illustrated in Fig. 1. First a 2000 Å thick Au layer was patterned (by lift-off) into a dumbbell shape of the collector. This layer was then used as an etch mask. The key processing step involved evaporation of self-aligned source/drain metal which provides ohmic contacts without degrading the integrity of the barrier. Devices reported in this work had $L_{CH} \times W = 1 \times 20\ \mu m^2$. Our use of a relatively heavy doping in the emitter channel ($5 \cdot 10^{17}\ cm^{-3}$) has resulted in a high yield and reproducibility, as well as higher RST current prior to the onset of instabilities associated with the channel NDR.

Figs. 2a and 2b show the static characteristics of the InP-barrier and InAlAs-barrier devices, respectively. InP-barrier devices show higher output current (I_C) at lower values of the heating and collector biases (V_D, V_C). This is explained by the lower conduction band discontinuity $\Delta E_C = 0.25\,eV$ in $In_{0.53}Ga_{0.47}As/InP$ heterojunction compared to $\Delta E_C = 0.5\,eV$ in $In_{0.53}Ga_{0.47}As/In_{0.52}Al_{0.48}As$ heterojunction [10], cf. Fig. 3, which leads to lower RST threshold in InP-barrier devices. At the same time, the leakage current of cold carriers (in the absence of a RST) is also higher in these devices. The transconductance $g_m = W^{-1}\,\partial I_C/\partial V_D$ has similar values for both devices, reaching 1.1 S/mm in the range of biases investigated.

We characterized the high-frequency operation of CHINT using a vector network analyzer. The device was operated in the common-source configuration with the input signal applied to the drain and the output taken from the collector. Scattering parameters were measured from 100 MHz to 40 GHz. Pad parasitics were removed by subtracting the Y-parameters of a pad without a device from the Y-parameters of the measured device. Frequency dependence of the magnitude of short-circuit current gain $|h_{21}|$, the power gain MAG/MSG, and the unilateral gain G_{Tu}^{max} are shown in Figs. 4. MAG is plotted when the stability factor $K > 1$, and for $K < 1$ MSG is plotted.

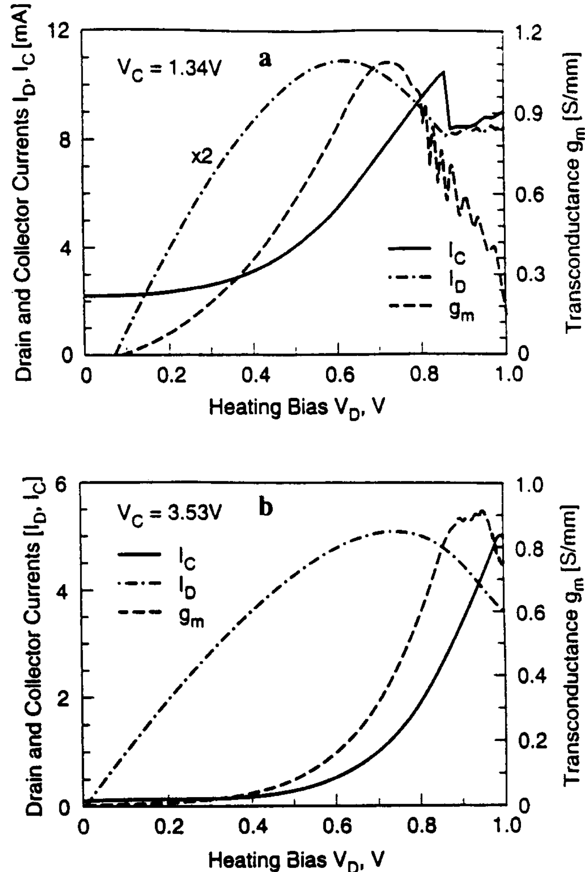

Fig. 2: Room temperature characteristics of the collector-up CHINT at a constant collector bias V_C: (a) InP barrier, (b) InAlAs barrier.

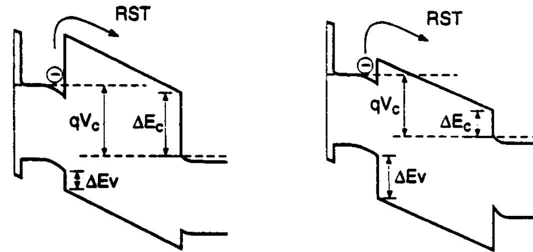

Fig. 3: Band diagram of a device cross-section near the source under a positive bias applied to the collector. The left half of the figure describes the $In_{0.53}Ga_{0.47}As/In_{0.52}Al_{0.48}As/In_{0.53}Ga_{0.47}As$ heterostructure and the right half the $In_{0.53}Ga_{0.47}As/InP/In_{0.53}Ga_{0.47}As$ heterostructure.

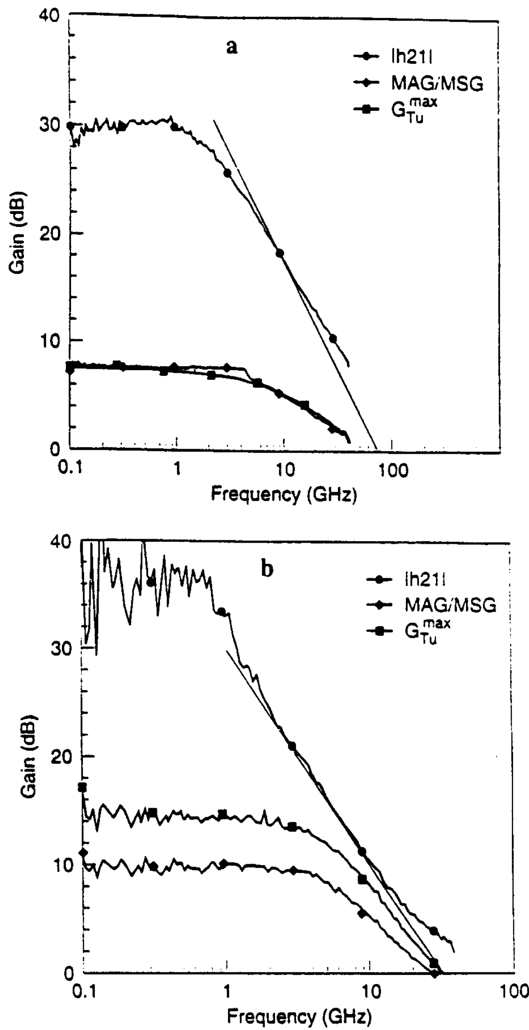

Fig. 4: Small-signal gain parameters at room temperature, calculated from the measured *S*-parameters at the following DC bias configurations: (a) InP barrier devices, $V_C = 1.34\,V$, $V_D = 0.61\,V$; (b) InAlAs-barrier device, $V_C = 3.53\,V$, $V_D = 0.75\,V$. Solid lines correspond to the extrapolation at -20 dB/decade.

For InP barrier devices (Fig. 4a) we found $f_T = 73$ GHz, obtained by extrapolating the data at -20 dB/decade through the point of least deviation of the measured slope from -20 dB/dec. This gives a very conservative estimate: the actual slope is only 16.5 dB/dec and extrapolating the curve at this slope would give a cutoff of 115 GHz. At 40 GHz the measured $|h_{21}| = 8$ dB and the power gain is larger than unity. In InAlAs-barrier devices (Fig. 4b), the steepest slope is actually -20 dB/dec; extrapolation at this slope gives $f_T = f_{max} = 32$ GHz. It should be noted, however, that at 40 GHz the measured $|h_{21}|$ is still > 1.

Quasi-static characteristics of the device strongly depend on the heating bias V_D and weakly on the collector bias V_C. A three-dimensional plot of $|h_{21}(V_D, V_C)|$ measured at 700 MHz is presented in Fig. 5 for the case of InAlAs barrier (the case of InP barrier is similar). A variation in V_D as small as 10 mV near the DC current gain maximum changes $|h_{21}|$ by more than 10 dB within the entire quasi-static band of about 1 GHz. At the same time, the f_T changes little if at all, because the slope of $|h_{21}(f)|$ peaks sharply at the same V_D, cf. Fig. 6. This extreme sensitivity of $|h_{21}|$ to quasi-static DC bias may find useful applications.

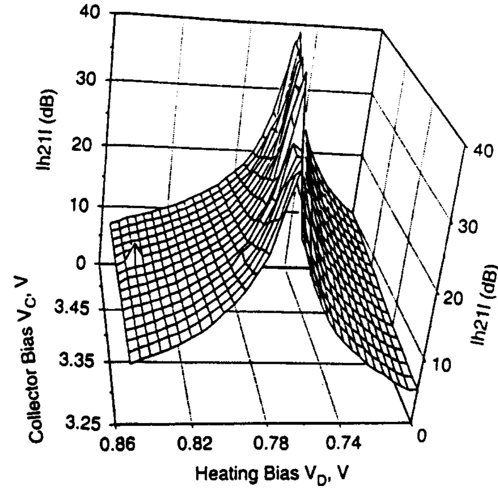

Fig. 5: Dependence of the quasi-static ($f = 700$ MHz) short-circuit current gain $|h_{21}|$ on the DC bias conditions for the InAlAs-barrier device.

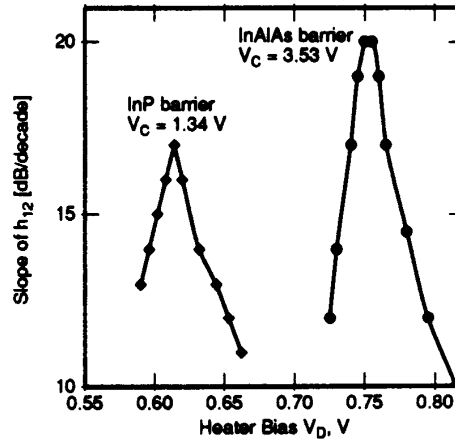

Fig. 6: Variation of the high-frequency slope $\partial|h_{21}|/\partial f$, measured at the point of its least deviation from -20 dB/dec, with the heating bias V_D at a constant collector bias V_C.

Discussion

We have found that InP-barrier devices show more than twice larger f_T than devices with InAlAs barrier, fabricated with the help of same mask set and virtually identical process. It should be further noted that our InAlAs barrier is about twice narrower than InP barrier. Let us discuss the possible origin of this significant difference in performance.

One of the fundamental speed limits in CHINT is due to the finite time of flight τ_F of electrons across the barrier. In order to ascribe our present results to this limitation, one would have to assume that the average velocity of carriers in InAlAs barrier is more than 4 times slower than that in InP barrier. This assumtpion does not seem to be plausible if we compare the generally accepted [11] values of peak and saturation velocities in InAlAs ($1.8 \cdot 10^7$, $4 \cdot 10^6$ cm/s) and InP ($2.3 \cdot 10^7$, $1 \cdot 10^7$ cm/s). The possibility of a nonequilibrium transport effect (like overshoot) favoring InP neither appears to us likely, since at the bias configuration of our microwave measurements the electric field across the barrier has been much larger in InAlAs devices.

We believe that the different microwave performance is likely to be explained by intervalley scattering effects manifesting themselves differently in the two materials, due to the difference in their heterojunction lineups (Fig. 3). Indeed, the satellite valley separation in InGaAs ($E_{\Gamma L} = 0.55$ eV [12]), which determines the threshold for intervalley scattering, is comparable in InAlAs-barrier devices to the conduction band discontinuity $\Delta E_C = 0.5$ eV [10], which determines the RST threshold. This means that a large fraction of hot electrons in InGaAs with energies above ΔE_C actually reside in L valleys. These electrons cannot go across the barrier because the L valley position in InAlAs is still much higher ($E_{\Gamma L} = 0.35$ eV [11]). Therefore, the RST in InGaAs/InAlAs depends on the establishment of a hot-electron equilibrium between Γ and L valleys and may be substantially slowed down by this process. This interpretation is in agreement with the discussion by Kizillyalli and Hess [6]. In contrast, in InP barrier devices, where the RST threshold is substantially lower, $\Delta E_C = 0.25$ eV $\approx 0.5\, E_{\Gamma L}$ (InGaAs), intervalley scattering is not likely to be important.

Acknowledgements

We are grateful to R. K. Montgomery for helpful discussions and T. R. Fullowan for silicon nitride deposition.

References

1. A. Kastalsky and S. Luryi, "Novel real-space transfer hot-electron transfer devices", *IEEE Electron Device Lett.* EDL-4, pp. 334-336 (1983); S. Luryi, A. Kastalsky, A. C. Gossard, and R. H. Hendel, "Charge injection transistor based on real-space hot-electron transfer", *IEEE Trans. Electron Dev.* ED-31, pp. 832-839 (1984).
2. A. Kastalsky, J. H. Abeles, R. Bhat, W. K. Chan, and M. Koza, *Appl. Phys. Lett.* 48, pp. 71-73 (1986).
3. P. M. Mensz, H. Schumacher, P. A. Garbinski, A. Y. Cho, D. L. Sivco, and S. Luryi, "Microwave operation of InGaAs/InAlAs charge injection transistors", *1990-IEDM Tech. Digest*, pp. 323-326 (1990).
4. M. R. Hueschen, N. Moll, and A. Fischer-Colbrie, "Improved microwave performance in transistors based on real-space electron transfer", *Appl. Phys. Lett.* 57, pp. 386-388 (1990).
5. K. Maezawa and T. Mizutani, "High-frequency characteristics of charge-injection transistor-mode operation in AlGaAs/InGaAs/GaAs metal-insulator-semiconductor field-effect transistors", *Jpn. J. Appl. Phys.* 30, pp. 1190-1193 (1991).
6. I. C. Kizillyalli and K. Hess, "Physics of Real-Space Transfer Transistors", *J. Appl. Phys.* 65, pp. 2005-2013 (1989).
7. T. Akeyoshi, K. Maezawa, M. Tomizawa, and T. Mizutani, "Monte Carlo study of charge injection transistors (CHINTs)", *Jpn. J. Appl. Phys.* 32, pp. 26-30 (1992).
8. M. B. Patil, U. Ravaioli, and M. R. Hueschen, "Monte Carlo simulation of real-space transfer transistors: device physics and scaling effect", *IEEE Trans. Electron Dev.* ED-40, pp. 480-486 (1993).
9. G. L. Belenky, P. A. Garbinski, S. Luryi, M. Mastrapasqua, A. Y. Cho, R. A. Hamm, T. R. Hayes, E. J. Laskowski, D. L. Sivco, and P. R. Smith, "Collector-Up Light-Emitting Charge Injection Transistors in n-InGaAs/InAlAs/p-InGaAs and n-InGaAs/InP/p-InGaAs Heterostructures", *J. Appl. Phys.* 73, pp. 8618-8627 (1993).
10. E. T. Yu, J. O. McCaldin and T. C. McGill, "Band offsets in semiconductor heterojunctions", in *Solid State Physics* 46, ed. by H. Ehrenreich and D. Turnbull (Academic Press, Boston, 1992) pp. 41-49.
11. H. S. Kim, H. Tian, K. W. Kim, and M. A. Littlejohn, "Electron velocity-field characteristics of $In_{0.52}Al_{0.48}As$", *Appl. Phys. Lett.* 61, 1202-1204 (1992).
12. S. Adachi, *Physical Properties of III-V Semiconductor Compounds*, Wiley-Interscience, New York (1992).